AN EFFICIENT MODEL FOR NUMERICAL ANALYSES IN NONLINEAR SOLID MECHANICS

Alexandre Luis Braun, allbraun@ig.com.br
Armando Miguel Awruch, amawruch@ufrgs.br
Programa de Pós-Graduação em Engenharia Civil – PPGEC
Universidade Federal do Rio Grande do Sul – UFRGS
Av. Osvaldo Aranha, 99, 3º andar, CEP 90035-190, Porto alegre –RS, Brasil

Abstract. An efficient numerical model to analyze problems on Nonlinear Solid Mechanics is presented in this work. It is well known that static analyses of solid bodies and structures with nonlinear behavior are usually carried out using the incremental approach and Newton-Raphson iterations in order to obtain equilibrium configurations during the load steps. Consequently, the computational costs associated to this kind of analysis are generally high when numerical models based on the Finite Element Method (FEM) are adopted. The key procedures of a static nonlinear algorithm are related to evaluations of the gradient matrix and stress state at element level, which must be updated at every iterative step. In addition, the constitutive relation must be also integrated during the iterative process if a nonlinear material is considered. Obviously, these computations are multiplied by the number of Gauss points needed for an exact integration of all the element matrices in a FEM formulation. In the present model, eight-node hexahedral elements with one-point quadrature are utilized to discretize the spatial field without excessive computations. The equilibrium equation is written in the rate form and a corrotational formulation is adopted for kinematical description of the continuum. Loads are applied using load subincrementation, where a coarse load increment is initially defined by the user, which may be automatically divided by the algorithm into smaller subincrements according to an error estimate based on the difference between first and second order displacement solutions. An explicit algorithm for integration of elastoplastic constitutive models is employed, where strain increments are divided into subincrements by using a subincrementation procedure similar to that utilized for the load increments. Some classical numerical examples are analyzed to demonstrate the efficiency and accuracy of the present formulation.

Keywords*: Finite Element Method (FEM), Nonlinear analysis, One-point quadrature*

1. INTRODUCTION

Although the linear behavior hypothesis can be considered as a reasonable approximation for many situations in the field of Solid Mechanics, it is well known that nonlinearities play an important role for most of the practical problems. These nonlinearities may be associated to geometrical or physical characteristics of the body analyzed, or a combination of both. Depending on the kind of nonlinearity observed, different approaches may be assumed to describe the problem analytically, which are basically related to the kinematical description of the continuum as well as the constitutive formulation of the material (see Belytschko et al., 2000).

The nonlinear problem is usually solved using the incremental approach with linearizations performed by taking into account the Newton-Raphson method (see Bathe, 1996). However, geometrically nonlinear analysis may present limit points related to snapping response of structures, where failures to achieve convergence are generally observed when a classical Newton-Raphson iterative procedure is adopted. Moreover, special characteristics are verified if the numerical model is developed using the Finite Element Method (FEM). The stiffness matrix and the internal force vector require periodic updates and the stress field must be evaluated employing energetically conjugated stress-strain measures at every iterative step. Since matrices and vectors derived from the application of the FEM are usually obtained considering numerical integration with the Gauss-Legendre quadrature, the computational efforts concerning all evaluations inherent to the method are multiplied by the number of quadrature points required for an exact representation of the geometrical field, which is also referred to as full quadrature. In this sense, finite elements utilizing one-point quadrature are very useful for nonlinear analysis, despite the additional numerical requirements related to element stabilization (see, for instance, Liu et al., 1998).

The classical Newton-Raphson method is based on iterative evaluations of the residual force vector, which consists in the difference between the external and internal force vectors. The stiffness matrix may be obtained considering displacement fields related to iterative or equilibrium states during the load steps, although the load is generally kept constant during iterations. These alternative procedures are referred to as full and modified Newton-Raphson method, respectively. Unfortunately, they may not converge owing to numerical difficulties associated to limit points or situations where the stiffness matrix changes by orders of magnitude. Therefore, various techniques have been developed to stabilize Newton-Raphson schemes, where the arc-length methods are the most popular.

In arc-length methods, the Newton-Raphson iterations are forced to remain near the last converged equilibrium point, such that load and displacement increments are dynamically adjusted along the equilibrium iterations in order to deal with limit points. The basic arc-length concepts were introduced by Wempner (1971), Riks (1972, 1979) and Crisfield (1981) and many contributions have been proposed since then. A review on the subject may be found in Memon and Su (2004).

The solution of the nonlinear equilibrium equation is usually obtained by dividing the total load into a number of load increments, where the magnitude of the load increments is defined considering a trial and error process. However, the size of the increments may vary by several orders of magnitude during the analysis, which is generally associated to the level of nonlinearity observed in the displacement response. In a subincrementation scheme, the load step is defined taking into account an estimate of the local error based on the difference between first and second order solutions of the equilibrium equation (Sloan and Abbo, 1999). Consequently, the load increments can be dynamically adjusted considering the local error estimate and a specific tolerance criterion based on an admissible error level. The numerical procedure is started considering a prescribed load step defined by the user, which must be large enough in order to reproduce the displacement response efficiently when the linear behavior is more evident.

Materials presenting physically nonlinear behavior require integration of the constitutive equation to obtain new stress states (see Owen and Hinton, 1980; Souza Neto et al., 2008). Methods for integrating the stress-strain relation are classified as explicit or implicit, where the former method is characterized by numerical schemes for which the yield surface, plastic potential gradients and hardening law are evaluated at known stress states and iterations are not necessary to predict the new stress state. On the other hand, in an implicit scheme, the new stress states are obtained by solving a system of nonlinear equations iteratively, which automatically satisfies the yield criterion for a specified tolerance value, considering that the hardening law and gradients are evaluated at unknown stress states. Furthermore, implicit schemes do not require a special algorithm to search the intersection point of the stress path on the yield surface during elastic-plastic transitions. However, explicit models are more attractive for a general purpose algorithm that can be applied to different constitutive formulations, since they require only first derivatives of the yield and plastic potential functions. Efficiency and accuracy can be also improved by using an automatic subincrementation scheme with error control, where the strain increment imposed by the solution of the equilibrium equation may be splitted into subincrements according to an estimate of the local error in the stress states (Sloan et al. 2001). Although explicit models can obtain the new stress states without solving a system of nonlinear equations, they need an additional step related to the evaluation of intersection points on the yield surface during elastic-plastic transitions.

It is well known that some of the most important characteristics of a finite element model are associated to convergence and numerical stability, which can be achieved when mesh refinement and the full quadrature technique are utilized. Nevertheless, finite element formulations with full quadrature are very inefficient, especially if three-dimensional nonlinear analyses are carried out, because evaluations of the stiffness matrix as well as the internal force vector require many computational operations. In addition, volumetric locking and shear locking may arise whether incompressible/nearly incompressible materials and thin structures under dominant bending are analyzed. In order to overcome those drawbacks, reduced integration and numerical techniques for hourglass control have been proposed, leading to explicit evaluations of the stiffness matrix and suppression of spurious modes that may be excited when full quadrature is not adopted. Finite element formulations for eight-node hexahedral elements with one-point quadrature were presented by Hu and Nagy (1997) and Duarte Filho and Awruch (2004), where a corotational system is employed to eliminate shear locking and for the kinematical description of the continuum. A comprehensive study on reduced integration applied to hexahedral elements may be found in Liu et al. (1998).

In the present work, a numerical model for linear and nonlinear static analysis of solid bodies is presented. A FEM formulation for eight-node hexahedrals with one-point quadrature is described, where the stiffness matrix can be analytically evaluated taking into account an accurate element stabilization procedure to eliminate hourglass and locking phenomena. The equilibrium equation is formulated considering a corotational system for the kinematical description of the continuum and a subincrementation scheme is employed in order to apply loads incrementally and efficiently. An explicit algorithm for integration of the constitutive equation is utilized, where strain increments are divided into subincrements by using a subincrementation scheme similar to that employed for the load increments. Some numerical applications are analyzed in order to validate the present model.

2. ANALYTICAL MODEL

Considering a classical Lagrangian kinematical description in the Cartesian coordinate system and in the absence of temperature changes and inertial forces, the conservation equations are reduced to the following expressions:

$$\int_{\Omega_0} \rho(\mathbf{X}, t_0)\, \mathrm{d}\Omega = \int_{\Omega} \rho(\mathbf{x}, t)\, \mathrm{d}\Omega \tag{1}$$

$$\nabla^{\mathrm{T}}\boldsymbol{\sigma} + \mathbf{b} = 0 \qquad \text{in } \Omega \tag{2}$$

where $\mathbf{X}$ and $\mathbf{x}$ are vectors containing components of the material (X_i) and spatial (x_i) coordinates in the Cartesian coordinate system, respectively, t represents time, ρ is the specific mass, ∇ is the differential operator, $\mathbf{b}$ is the body force vector and $\boldsymbol{\sigma}$ is the Cauchy stress tensor. It is important to notice that the equilibrium equation, which is derived from the Cauchy's equation of motion, is defined taking into account the current deformed configuration of the body (Ω).

In the present work, a linear hypoelastic constitutive model is adopted in order to relate strain and stress measures in the elastic regime, which may be described as follows:

$$\boldsymbol{\sigma} = \mathbf{D}^{\mathrm{e}}\boldsymbol{\varepsilon} \tag{3}$$

where $\boldsymbol{\varepsilon}$ is the infinitesimal strain tensor and:

$$\mathbf{D}^{e} = \begin{bmatrix} K+\frac{4}{3}G & K-\frac{2}{3}G & K-\frac{2}{3}G & 0 & 0 & 0 \\ & K+\frac{4}{3}G & K-\frac{2}{3}G & 0 & 0 & 0 \\ & & K+\frac{4}{3}G & 0 & 0 & 0 \\ & \textit{symm.} & & G & 0 & 0 \\ & & & & G & 0 \\ & & & & & G \end{bmatrix} \tag{4}$$

where K and G are the bulk and shear moduli, respectively, given as follows:

$$K = \frac{E}{3(1-2\nu)} \tag{5}$$

$$G = \frac{E}{2(1+\nu)} \tag{6}$$

where E is the Young's modulus and ν is the Poisson's ratio. The bulk modulus associates spherical pressures with volumetric strains while the shear modulus associates deviatoric stresses with deviatoric strains.

When infinitesimal displacements and rotations are observed, the geometrical linear approach can be utilized, where the undeformed configuration of the body is taken as reference throughout the analysis. In addition, the Cauchy stress tensor and the infinitesimal strain tensor are adopted in order to describe the stress-strain relation. On the other hand, when displacements and rotations are large, a special treatment must be considered in order to obtain accurate results for the strain field. The equilibrium equation may be written in terms of the undeformed or current configurations, depending on the formulation utilized for the kinematical description of the continuum.

Although the total and updated Lagrangian formulations are commonly utilized in the field of solid mechanics, a corotational formulation is employed in this work, where a local coordinate system is embedded to every element of the finite element mesh (see Belytschko et al., 2000). The corotational coordinate system may be defined as a Cartesian coordinate system that rotates along with the element, leading to stress measures that are not affected by rigid body motions. Moreover, considering that the finite element discretization is fine enough, the motion of the continuum can be decomposed locally into rigid body motion and pure deformation. When the rigid body motion is eliminated from the displacement field, which corresponds to large displacements and rotations and small strains in the present work, the portion related to pure deformation will be a small quantity when compared to the element size. Therefore, the Cauchy stress tensor and the small strain tensor defined in the corotational coordinate system can be utilized in the constitutive equation (see Eq. (3)).

In order to maintain objectivity over the stress measures in the corotational coordinate system for incremental formulations, the Truesdell rate tensor is adopted here to calculate stress increments, which may be written as:

$$\Delta\hat{\boldsymbol{\sigma}}^{\mathbf{TR}} = \Delta\hat{\boldsymbol{\sigma}} - \Delta\mathbf{L}\,\hat{\boldsymbol{\sigma}} - \hat{\boldsymbol{\sigma}}\,\Delta\mathbf{L}^{\mathbf{T}} + \hat{\boldsymbol{\sigma}}\,\mathrm{tr}\Delta\hat{\boldsymbol{\varepsilon}} \tag{7}$$

where $\hat{\boldsymbol{\sigma}}$ is the Cauchy stress tensor defined in the corotational coordinate system and $\Delta\mathbf{L}$ is the increment of the velocity gradient tensor in the corotational coordinate system, which may be decomposed into symmetric and skew-symmetric parts by:

$$\Delta\mathbf{L} = \Delta\hat{\boldsymbol{\varepsilon}} + \Delta\hat{\boldsymbol{\omega}} \tag{8}$$

where $\Delta\hat{\boldsymbol{\varepsilon}}$ and $\Delta\hat{\boldsymbol{\omega}}$ are increments of the strain rate and spin rate tensors, respectively. These increments are obtained by assuming that the velocity vector ($\dot{\mathbf{u}}$) is constant during the time interval $[t_n, t_{n+1}]$, i.e.:

$$\Delta\hat{\boldsymbol{\varepsilon}} = \int_{t_n}^{t_{n+1}} \dot{\boldsymbol{\varepsilon}}\,d\tau = \frac{1}{2}\left[\frac{\partial\Delta\hat{\mathbf{u}}}{\partial\hat{\mathbf{x}}_{n+1/2}} + \left(\frac{\partial\Delta\hat{\mathbf{u}}}{\partial\hat{\mathbf{x}}_{n+1/2}}\right)^{T}\right] \tag{9}$$

$$\Delta\hat{\boldsymbol{\omega}} = \int_{t_n}^{t_{n+1}} \dot{\boldsymbol{\omega}}\,d\tau = \frac{1}{2}\left[\frac{\partial\Delta\hat{\mathbf{u}}}{\partial\hat{\mathbf{x}}_{n+1/2}} - \left(\frac{\partial\Delta\hat{\mathbf{u}}}{\partial\hat{\mathbf{x}}_{n+1/2}}\right)^{T}\right] \tag{10}$$

where $\Delta\hat{\mathbf{u}}$ is the displacement increment referred to the corotational coordinate system and $\hat{\mathbf{x}}_{n+1/2}$ is the intermediate configuration of the body defined in the corotational coordinate system and within the time interval $[t_n, t_{n+1}]$, which are obtained from the following objective transformations:

$$\Delta\hat{\mathbf{u}} = \hat{\mathbf{x}}_{n+1} - \hat{\mathbf{x}}_{n} = \mathbf{R}_{n+1}\mathbf{x}_{n+1} - \mathbf{R}_{n}\mathbf{x}_{n} \tag{11}$$

$$\hat{\mathbf{x}}_{n+1/2} = \mathbf{R}_{n+1/2}\mathbf{x}_{n+1/2} = \frac{1}{2}\mathbf{R}_{n+1/2}\left(\mathbf{x}_{n} + \mathbf{x}_{n+1}\right) \tag{12}$$

where $\hat{\mathbf{x}}$ and $\mathbf{x}$ represents body configurations in the corotational and global coordinates system, respectively, which are defined with respect to their positions in the time interval and are denoted by the subindices. The rotation matrix $\mathbf{R}$ is also defined considering a specific position within the time interval $[t_n, t_{n+1}]$. In the present work, a simple procedure for obtaining the rotation matrix is utilized according to the paper presented by Belytschko and Bindeman (1993).

Once the stress and strain tensors are defined in the corotational coordinate system, the stiffness matrix and the internal force vector will be also referenced to the same coordinate system. In order to solve the system of equilibrium equations in the global coordinate system, the stiffness matrix and the internal force vector must be submitted to the following objective transformations:

$$\mathbf{K} = \mathbf{R}^{\mathrm{T}}\hat{\mathbf{K}}\mathbf{R} \tag{13}$$

$$\mathbf{f}^{\mathbf{int}} = \mathbf{R}^{\mathrm{T}}\hat{\mathbf{f}}^{\mathbf{int}} \tag{14}$$

where $\mathbf{K}$ and $\mathbf{f}^{\mathbf{int}}$ are the stiffness matrix and the internal force vector defined in the global coordinate system and $\hat{\mathbf{K}}$ and $\hat{\mathbf{f}}^{\mathbf{int}}$ are the stiffness matrix and the internal force vector defined in the corotational coordinate system. Further information about the corotational formulation employed in this work may be found in Duarte Filho and Awruch (2004) and Braun and Awruch (2008).

In the elastoplastic range, a yield function f, a plastic potential g, a flow rule and a hardening law must be introduced in order to define the elastoplastic formulation (see Owen and Hinton, 1980). The yield function for the von Mises criterion is employed in the present work, which may be written as (Souza Neto et al., 2008):

$$f(\boldsymbol{\sigma}) = \sqrt{J_2} - \frac{\sigma_y}{\sqrt{3}} \tag{15}$$

where J_2 ($J_2 = \frac{1}{2}\mathbf{s}:\mathbf{s}$) is the second invariant of the deviator stress tensor $\mathbf{s}$ ($\mathbf{s} = \boldsymbol{\sigma} - \frac{1}{3}(\mathrm{tr}\,\boldsymbol{\sigma})\mathbf{I}$) and σ_y is the uniaxial yield stress.

Since the constitutive equation may become nonlinear in the elastoplastic range, an incremental approach must be adopted to define the stress-strain relations during the stress path, i.e.:

$$\mathrm{d}\boldsymbol{\sigma} = \mathbf{D}^{\mathbf{ep}}\mathrm{d}\boldsymbol{\varepsilon} \tag{16}$$

with:

$$\mathbf{D}^{\mathbf{ep}} = \mathbf{D}^{\mathbf{e}} - \frac{\mathbf{D}^{\mathbf{e}}\mathbf{a}_{\mathbf{g}}\mathbf{a}_{\mathbf{f}}^{\mathrm{T}}\mathbf{D}^{\mathbf{e}}}{A + \mathbf{a}_{\mathbf{f}}^{\mathrm{T}}\mathbf{D}^{\mathbf{e}}\mathbf{a}_{\mathbf{g}}}\mathrm{d}\boldsymbol{\varepsilon} \tag{17}$$

where A is the hardening parameter and $\mathbf{a}_{\mathbf{f}}$ and $\mathbf{a}_{\mathbf{g}}$ are flow vectors based on the yield and plastic potential functions, respectively. For materials with linear isotropic hardening, $A = h$, where h is the hardening modulus. By assuming an associative flow rule, where $f \equiv g$, $\mathbf{a}_{\mathrm{g}}$ and $\mathbf{a}_{\mathrm{f}}$ lead to the same result.

2. NUMERICAL MODEL

Applying the Bubnov-Galerkin weighted residual method in conjunction with the Green-Gauss theorem over the momentum equation (Eq. 2), the following expression is obtained:

$$\sum_{\mathrm{E}=1}^{\mathrm{nel}}\left(\int_{\Omega_{\mathrm{E}}}(\nabla\delta\mathbf{u})^{\mathrm{T}}\,\boldsymbol{\sigma}\,\mathrm{d}\Omega_{\mathrm{E}}\right) = \sum_{\mathrm{E}=1}^{\mathrm{nel}}\left(\int_{\Omega_{\mathrm{E}}}\delta\mathbf{u}^{\mathrm{T}}\mathbf{b}\,\mathrm{d}\Omega_{\mathrm{E}} + \int_{\Gamma_{\mathrm{E}}}\delta\mathbf{u}^{\mathrm{T}}\mathbf{t}\,\mathrm{d}\Gamma_{\mathrm{E}}\right) \tag{18}$$

where $\mathbf{t}$ is the traction vector and Ω_{E} and Γ_{E} are the volume and the boundary surfaces referred to element E, respectively, with both considered in the FEM context. The total number of elements utilized in the spatial discretization is indicated by *nel*.

Spatial coordinates and displacements are approximated at element level using the eight-node hexahedral finite element formulation (see, for instance, Belytschko et al., 2000). The final matrix format of the equilibrium equation is obtained by introducing the finite element approximations for the spatial and variable fields into Eq. (18), which may be represented, considering an incremental/iterative approach based on the Newton-Raphson linearization, as follows:

$$\mathbf{K}^{\tan}_{\mathrm{n+1,i-1}}(\mathbf{u},\boldsymbol{\sigma})\Delta\mathbf{u}_{\mathrm{n+1,i}} = \mathbf{f}^{\mathrm{ext}}_{\mathrm{n+1}} - \mathbf{f}^{\mathrm{int}}_{\mathrm{n+1,i-1}}(\mathbf{u},\boldsymbol{\sigma}) \tag{19}$$

where subscripts $n + 1$ denote current position in the time marching with i and i-1 indicating current and previous iterative steps in the Newton-Raphson method. The vector of external forces $\mathbf{f}^{\mathrm{ext}}$ represents the right-hand side terms of Eq. (18), while $\mathbf{K}^{\tan}$ and $\mathbf{f}^{\mathbf{int}}$ are related to the tangent stiffness matrix and the internal force vector, respectively. The tangent stiffness matrix and the internal force vector are evaluated in the corotational coordinate system using the following expressions:

$$\hat{\mathbf{K}}^{\tan}_{\mathrm{n,i}} = \int_{\hat{\Omega}_{\mathrm{E}}}\hat{\mathbf{B}}^{\mathrm{T}}(\mathbf{D}+\mathbf{T})\hat{\mathbf{B}}\,\mathrm{d}\hat{\Omega}_{\mathrm{E}} \tag{20}$$

$$\hat{\mathbf{f}}_{\mathrm{n,i}} = \int_{\hat{\Omega}_{\mathrm{E}}}\hat{\mathbf{B}}^{\mathrm{T}}\hat{\boldsymbol{\sigma}}_{\mathrm{i}}\,\mathrm{d}\hat{\Omega}_{\mathrm{E}} \tag{21}$$

where $\hat{\Omega}_E$ refers to the current element configuration in the corotational system, **D** and **T** are fourth order tensors related to the elastic constitutive equation and Truesdell rate terms, respectively, and $\hat{\boldsymbol{\sigma}}_i$ is the corotational Cauchy stress tensor evaluated at iterative step *i* (see Braun and Awruch, 2008 and Duarte Filho and Awruch, 2004 for further details). It is important to notice that **T** vanishes when geometrically linear problems are carried out as well as **D** becomes $\mathbf{D}^e$ for elastic materials and $\mathbf{D}^{ep}$ for elastoplastic materials. In order to solve the equilibrium equation, the tangent stiffness matrix and the internal force vector are brought back to the global coordinate system using objective transformations (see Eqs. 13 and 14).

Element formulations based on reduced integration must be stabilized using hourglass control techniques in order to avoid numerical instabilities. In this work, volumetric locking is remedied using reduced selective integration, where the gradient matrix $\hat{\mathbf{B}}$ defined in the corotational system is decomposed into deviatoric and volumetric terms of the strain tensor $\boldsymbol{\varepsilon}$, with the last terms evaluated at the center of the element. In addition, deviatoric terms must be expanded using Taylor series at the center of the element up to bilinear terms. The same procedure is carried out over the stress tensor $\boldsymbol{\sigma}$. On the other hand, shear locking is removed by describing shear components of the strain tensor $\boldsymbol{\varepsilon}$ in an orthogonal corotational coordinate system. Moreover, all shear components must be linearly interpolated in a single direction of the reference system. In order to evaluate the internal force vector accurately when distorted elements are considered, the gradient matrix obtained with reduced integration is replaced by uniform gradient submatrices defined by Flanagan and Belytschko (1981). Further details about the reduced integration scheme adopted in this paper may be found in Braun and Awruch (2008). See also Reese (2005) for element stabilization techniques considering three-dimensional finite elastoplasticity.

An automatic load stepping scheme is employed in this work in order to solve the system of nonlinear equilibrium equations. The present algorithm assumes that a coarse load increment is initially proposed by the user, which may be automatically splitted into a number of smaller load increments denominated subincrements according to the current characteristics of the nonlinear equilibrium equations. The coarse load step is defined in the fictitious time interval $[t_n; t_{n+1}]$, where Δt is the coarse load increment such that $\Delta t = t_{n+1} - t_n$. The subincrements h_i are assumed to be within the time interval $[t_n; t_{n+1}]$ and the load stepping procedure during subincrementation may be defined as $t_{i+1} = t_i + h_i$, where t_i is assumed to be t_n for the first subincrement h_1 and t_{i+1} must be equal to t_{n+1} for the last subincrement.

The size of the subincrements is defined considering an estimate of the local truncation error in the displacements field, which is based on the difference between first and second order approximations obtained from Taylor series expansions, i.e.:

$$\mathbf{E}_{i+1} = \mathbf{u}_{i+1}^{(2)} - \mathbf{u}_{i+1}^{(1)} = \frac{h^2}{2}\frac{\partial^2 \mathbf{u}_{i+1}}{\partial h^2} = \frac{h}{2}\Delta\dot{\mathbf{u}} = \frac{h}{2}\left[\left(\frac{\Delta\mathbf{u}}{h}\right)^{i+1} - \left(\frac{\Delta\mathbf{u}}{h}\right)^{i}\right] \tag{22}$$

where:

$$\mathbf{u}_{i+1}^{(2)} = \mathbf{u}_i + h\frac{\partial \mathbf{u}_{i+1}}{\partial h} + \frac{h^2}{2}\frac{\partial^2 \mathbf{u}_{i+1}}{\partial h^2} \tag{23}$$

$$\mathbf{u}_{i+1}^{(1)} = \mathbf{u}_i + h\frac{\partial \mathbf{u}_{i+1}}{\partial h} \tag{24}$$

with i denoting subincrements.

The error control scheme utilized in this work takes into account the relative error defined by Eq. (22) and the current displacement field $\mathbf{u}_{i+1}$, both obtained considering the last converged subincrement in the Newton-Raphson iterations. A dimensionless relative error is then given by:

$$R_{i+1} = \frac{|\mathbf{E}_{i+1}|}{|\mathbf{u}_{i+1}|} \tag{25}$$

The current subincrement is accepted if R_{i+1} lies below a specified tolerance error E_{tol} and rejected otherwise. In either case, the size of the next subincrement h_{i+1} is determined from:

$$h_{i+1} = qh_i \tag{26}$$

where h_i is the last load subincrement and:

$$q = 0.8\sqrt{E_{tol} / R_{i+1}} \tag{27}$$

considering an additional constraint defined as:

$$0.1 \le q \le 2 \tag{28}$$

which is imposed in order to prevent an excessive number of subincrements and an excessive growth of size during consecutive subincrements. Consequently, the size of the subincrements are limited according to:

$$h^{max} = \min(\Delta t, h, t_{n+1} - t_{i+1}) \tag{29}$$

The numerical algorithm to solve the nonlinear system of equilibrium equations may be summarized as follows:

a) For a specific load subincrement *h*, determine the displacement solution using the Newton Raphson method (see Eq. 19). If the solution fails to converge set $h = 0.25h$ and start over the iteration procedure.

b) After convergence, estimate the local truncation error using Eq. (25) and the tolerance error E_{tol}. In addition, determine the dot product between the current and last displacement rate increments ($\Delta\dot{\mathbf{u}}_i^T.\Delta\dot{\mathbf{u}}_{i+1}$) in order to identify limit points.

c) If $R_{i+1} > E_{tol}$ or $\Delta\dot{\mathbf{u}}_i^T.\Delta\dot{\mathbf{u}}_{i+1} < 0$ then the current subincrement has failed; estimate a smaller subincrement considering Eqs. (26), (27) and Eq. (28) and start over the iterative procedure (step a). If $\Delta\dot{\mathbf{u}}_i^T.\Delta\dot{\mathbf{u}}_{i+1} < 0$, set $h_{new} = -h_{new}$, where h_{new} is a new estimate for the load subincrement h.

d) If $R_{i+1} < E_{tol}$ and $\Delta\dot{\mathbf{u}}_i^T.\Delta\dot{\mathbf{u}}_{i+1} > 0$ then the current subincrement is accepted and a new displacement field can be computed using the incremental solution obtained from the Newton-Raphson iterative procedure (step a).

e) After the subincrement is accepted, estimate the size of the next subincrement taking into account Eqs. (26), (27) and the constraints defined by Eqs. (28) and (29). If the previous subincrement failed, set q = min (q, 1).

f) If $t_{i+1} = t_i + h_i$ is equal to $t_{n+1} = \Delta t + t_n$, then the integration of the current load step Δt is completed; set $t_i = t_{n+1}$ and proceed with the integration of the next load step (step a) until all the load steps are applied.

When elastoplastic analysis is carried out, strain increments $\Delta\boldsymbol{\varepsilon}$ are imposed at element level based on the incremental solution obtained from the equilibrium equation. On the other hand, stress increments are dependent on the material behavior. Therefore, a trial elastic stress increment is usually considered as an initial estimate for the new stress state. If this new stress state does not lead to plastic yielding, the corresponding stress increment is taken as true. However, if plastic yielding is observed, the following system of ordinary differential equations must be solved:

$$\frac{d\boldsymbol{\sigma}}{dT} = \mathbf{D}^{ep}\Delta\boldsymbol{\varepsilon} \tag{30}$$

$$\frac{d\kappa}{dT} = \Delta\lambda B \tag{31}$$

with:

$$T = \frac{t^* - t_0^*}{h} \tag{32}$$

$$\Delta\lambda = \frac{\mathbf{a}_f^T\mathbf{D}^e}{A + \mathbf{a}_f^T\mathbf{D}^e\mathbf{a}_g}\Delta\boldsymbol{\varepsilon} \tag{33}$$

$$B = -\frac{A}{\partial f/\partial\kappa} \tag{34}$$

where T is a dimensionless time parameter, which is defined in the range $0 \le T \le 1$, t_0^* is the artificial time at the starting point of the load subincrement (h), t^* is the artificial time in a position within the load subincrement (h), B is a hardening parameter, $d\kappa$ is the increment of the hardening parameter and f is the yield function.

Once the elastic part of the stress increment $\Delta\boldsymbol{\varepsilon}$ is obtained, the plastic part of the strain increment ($\Delta\boldsymbol{\varepsilon}'$) is determined using:

$$\Delta\boldsymbol{\varepsilon}' = (1-\alpha)\Delta\boldsymbol{\varepsilon} \tag{35}$$

and the stress state at the onset of the plastic yielding $\boldsymbol{\sigma}_{yld}$ is calculated from:

$$f(\boldsymbol{\sigma}_0 + \alpha\mathbf{D}^e\Delta\boldsymbol{\varepsilon}, \kappa_0) = 0 \tag{36}$$

where α is a scalar to be determined considering the yielding condition expressed by Eq. (36).

In order to define initial conditions for the system of equations described by Eqs. (30) and (31), the stress state $\boldsymbol{\sigma}_0$ is updated to the stress state at the onset of the plastic yielding $\boldsymbol{\sigma}_{yld}$ and the hardening parameter κ_0 is considered to be at the start of the strain increment $\Delta\boldsymbol{\varepsilon}'$, where T = 0 and $t^* = t_0^*$. By using the explicit Euler method, a substepping technique, as proposed by Sloan et al. (2001), is applied over the strain increment $\Delta\boldsymbol{\varepsilon}'$ to find the stress state and the hardening parameter at the end of $\Delta\boldsymbol{\varepsilon}'$, where T = 1. Subincrements of $\Delta\boldsymbol{\varepsilon}'$ are defined according to the dimensionless time increment ΔT, which is calculated taking into account a local error measure obtained from the difference between a second order accurate modified Euler solution and a first order accurate Euler solution. Consequently, the size of the subincrements is automatically modified along the integration process. For a complete description of the numerical algorithm utilized in this work to integrate the constitutive equation, see Sloan et al. (2001).

4. NUMERICAL APPLICATIONS

4.1 Geometrically nonlinear examples

In the present section, geometrically nonlinear analyses are carried out in order to investigate some numerical aspects related to the numerical algorithm presented in this work, where computational performance and accuracy are evaluated from the results obtained in the numerical simulations. Most of the simulations are also performed considering the linear hypothesis on the kinematical description of the continuum. Geometrical characteristics and

boundary conditions employed in the applications analyzed here are presented in Fig. 1 and the corresponding physical properties may be found in Table 1.

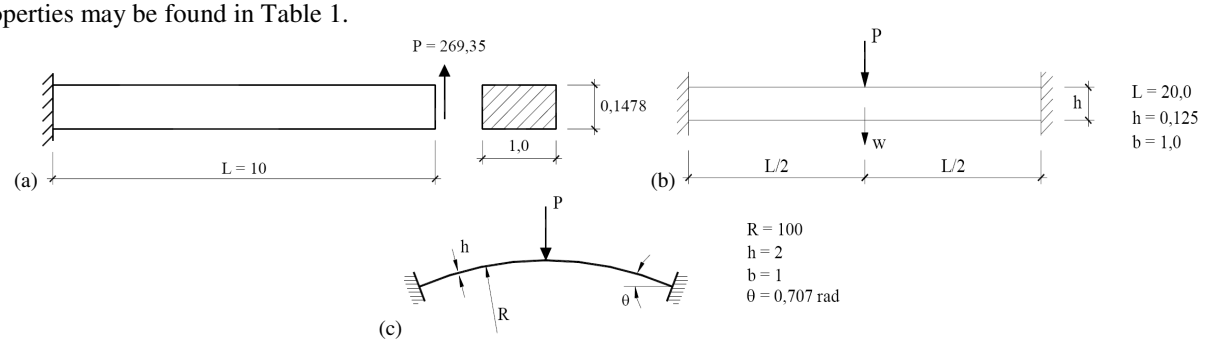

Figure 1. Geometrical characteristics and boundary conditions utilized in the geometrical nonlinear examples: (a) cantilever beam; (b) clamped beam; (c) clamped arch.

Table 1. Load and physical properties adopted in the geometrical nonlinear examples.

Mechanical properties	Numerical applications		
	Cantilever beam	Clamped beam	Clamped arch
Young's modulus – E [N/m^2]	1.0x10^8	3.0x10^7	1.0x10^7
Poisson's ratio - ν	0.00	0.00	0.25
Load – P [N]	269.35	640.00	2.0x10^4

A first analysis is carried out considering a cantilever beam submitted to a concentrated load applied conservatively at the free end. Results corresponding to vertical displacements at the free end are presented in Fig. 2a, where comparisons are performed using predictions obtained from a reference work (Duarte Filho, 2002) and predictions obtained with the numerical model proposed here. Different load factors (dimensionless loads obtained with respect to the total load P) were adopted to evaluate the influence of the load discretization over numerical results when nonlinear analyses are performed. One can verify that all responses obtained here agree very well with the numerical predictions obtained by Duarte Filho (2002), especially when the smaller load increments are considered. The linear response is also in accordance with the prediction obtained by Duarte Filho (2002).

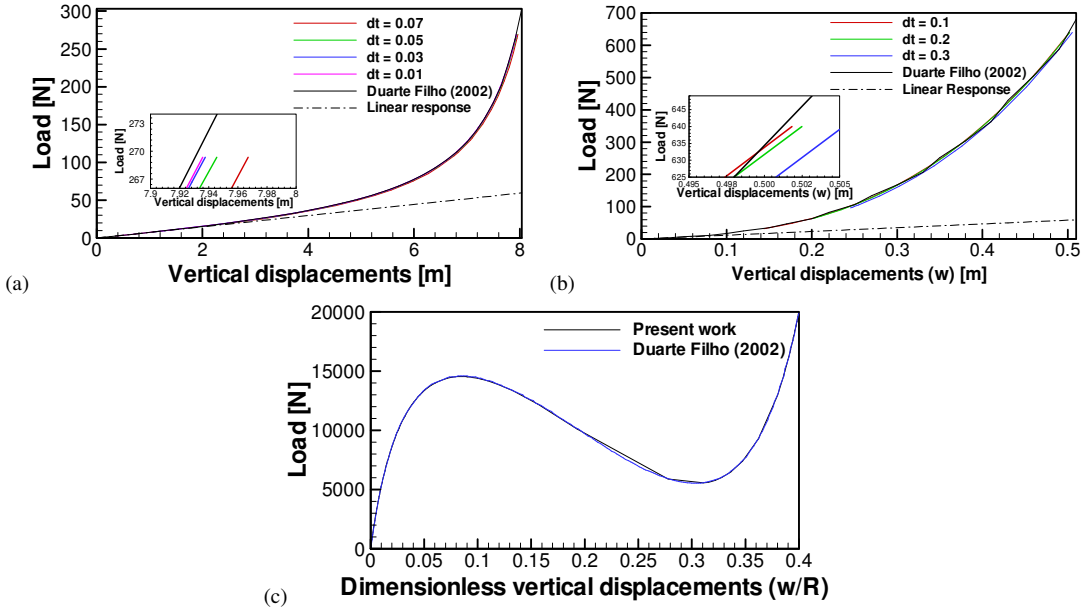

Figure 2. Displacement responses obtained in the geometrically nonlinear analyses: (a) cantilever beam; (b) clamped beam; (c) clamped arch.

A second investigation is performed considering now a clamped beam with a point load applied at the mid span. The predictions obtained with the present algorithm are found in Fig 2b, which are again referenced to different load increments adopted in the load discretization. In accordance with comparisons shown previously, the numerical model demonstrates here a good accuracy when compared to numerical predictions obtained by Duarte Filho (2002). One can also verify that the present predictions approximate the reference results as the load factors are reduced.

In order to observe the computational performance of the present model when problems with limit points are investigated, a geometrically nonlinear analysis is carried out considering a clamped arch submitted to a point load applied at the mid span. Vertical displacements measured at the location of the point load are presented in Fig. 2c,

where predictions obtained here are again compared with those obtained by Duarte Filho (2002). One can note that two limit points are found during the load application, which can be perfectly handled with the subincrementation procedure proposed in this work when $\Delta t = 0.01$ is considered.

Deformed configurations obtained during the geometrically nonlinear analyses performed for the clamped beam and the clamped arch are shown in Fig. 3, where the snap-back phenomenon can be easily identified for the clamped arch analysis (see Fig. 3b). The computational performance of the subincrementation procedure may be evaluated considering the number of Newton-Raphson iterations per load step obtained in the numerical analyses performed here, which is demonstrated in Fig. 4. It is observed that although the larger load steps present some difficulties to converge in the early stages of the numerical analysis, the number of iterations tend to stabilize for all the load steps analyzed as the load factor is increased.

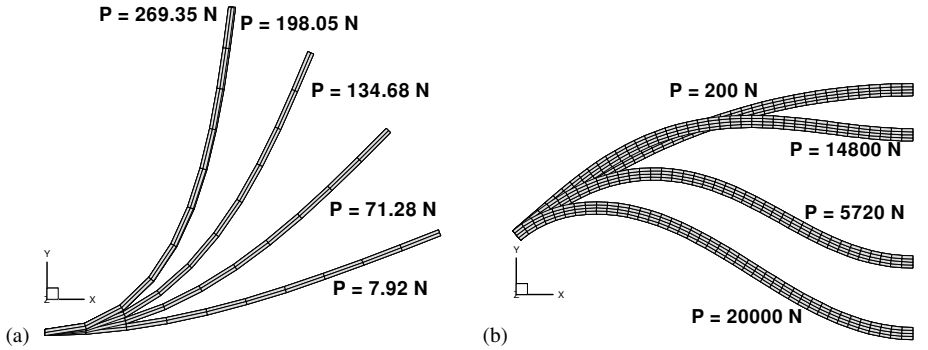

Figure 3. Deformed configurations obtained during the load application: (a) cantilever beam analysis; (b) clamped arch analysis.

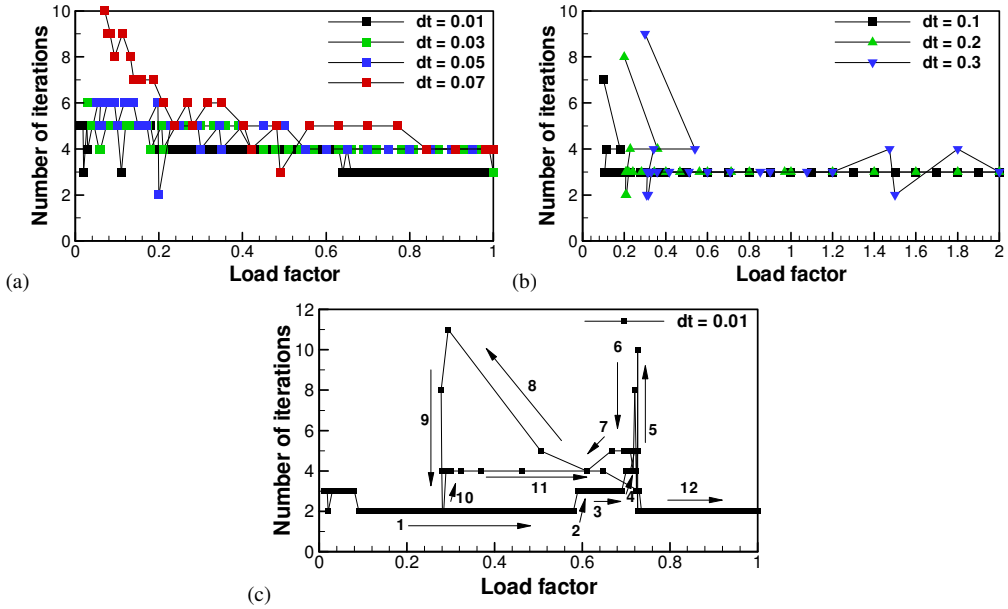

Figure 4. Computational performance obtained by the present model during the geometrically nonlinear analyses: (a) cantilever beam; (b) clamped beam; (c) clamped arch.

4.2 Physically nonlinear examples

Some examples are analyzed in this section to observe the performance of the numerical algorithm proposed in this work for physically nonlinear applications. The same numerical aspects investigated in the previous analyses are revisited here. Geometrical characteristics and boundary conditions utilized in the numerical analyses performed in the present study are shown in Fig. 5 and the corresponding physical properties are specified in Table 2.

Table 2. Load and physical properties adopted in the physically nonlinear examples.

Mechanical properties	**Numerical applications**		
	Unit cube	**Cantilever beam**	**Simply supported square plate**
Young's modulus – E [N/m^2]	$1.2\text{x}10^{7}$	$1.0\text{x}10^{7}$	$3.0\text{x}10^{10}$
Plastic modulus – E_T [N/m^2]	$1.2\text{x}10^{5}$	$1.0\text{x}10^{6}$	$3.0\text{x}10^{9}$
Uniaxial yield stress - σ_y [N/m^2]	$2.4\text{x}10^{4}$	$3.0\text{x}10^{5}$	$4.0\text{x}10^{7}$
Poisson's ratio - ν	0.0	0.3	0.3
Load – P [N]	$2.6\text{x}10^{4}$	$8.0\text{x}10^{4}$	$7.0\text{x}10^{4}$

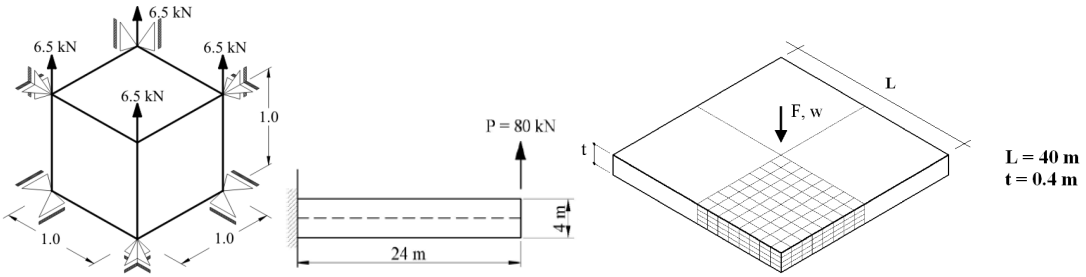

Figure 5. Geometrical characteristics and boundary conditions utilized in the physically nonlinear examples: (a) unit cube; (b) cantilever beam; (c) square plate.

A unit cube under axial load is analyzed considering the von Mises yield criterion (see Eq. 15) and geometrically nonlinear behavior. In Fig. 6a, results obtained here with $\Delta t = 0.05$ are compared to numerical predictions obtained by Schmidt (2006), where a perfect agreement is observed for vertical displacements measured at the top of the unit cube. A numerical analysis was also carried out considering the geometrically linear approach, which obtained the same accuracy when compared to the reference work.

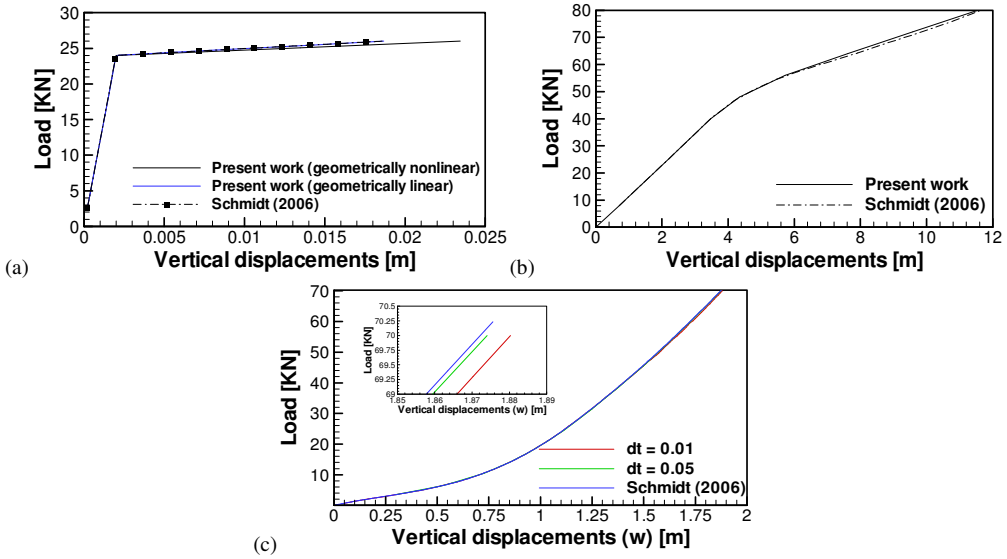

Figure 6. Displacement responses obtained in the physically nonlinear analyses: (a) unit cube; (b) cantilever beam; (c) square plate.

A cantilever beam is now analyzed considering a point load applied at the free end. The constitutive model assumes an elastoplastic behavior with the von Mises yield criterion and the kinematical description is performed using the geometrically nonlinear approach. In Fig. 6b, results corresponding to vertical displacements measured at the free end are presented, where predictions obtained with the numerical model proposed in this work and $\Delta t = 0.1$ are compared to those obtained numerically by Schmidt (2006). One can verify that a good agreement is observed, although some differences can be identified in the plastic range, which may related to the sensitivity of the subincrementation procedure to parameters adopted in the numerical integration of the constitutive equation (see Sloan et al., 2001 and Schmidt, 2006).

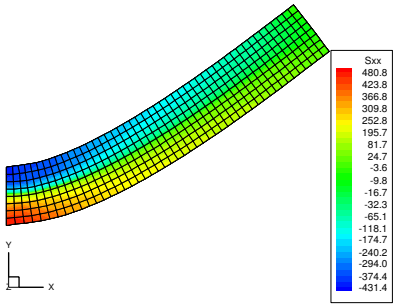

Figure 7. Final configuration and stress field $\boldsymbol{\sigma}_{xx}$ obtained for the cantilever beam analysis.

A square plate with all borders simply supported is analyzed considering a concentrated load applied at the center point. An elastoplastic behavior is assumed taking into account the von Mises yield criterion. In addition, the geometrically nonlinear approach is considered for the kinematical description of the continuum. Results concerning the vertical displacements observed at the center point are shown in Fig. 6c, where predictions obtained here are again

compared to those obtained by Schmidt (2006). The present simulations were performed with $\Delta t = 0.01$ and $\Delta t = 0.05$, both presenting a good agreement with the reference work.

The final configuration obtained in the cantilever beam analysis is shown in Fig. 7, where the stress field σ_{xx} is also presented. The computational performance is evaluated here considering the number of Newton-Raphson iterations per load step obtained in the numerical analyses performed in this section, where different load steps were investigated. In Fig. 8, one can observe that convergence may be reached even with large load steps, since the numerical scheme adopted in the present paper is able to split the load steps into subincrements whenever it is necessary.

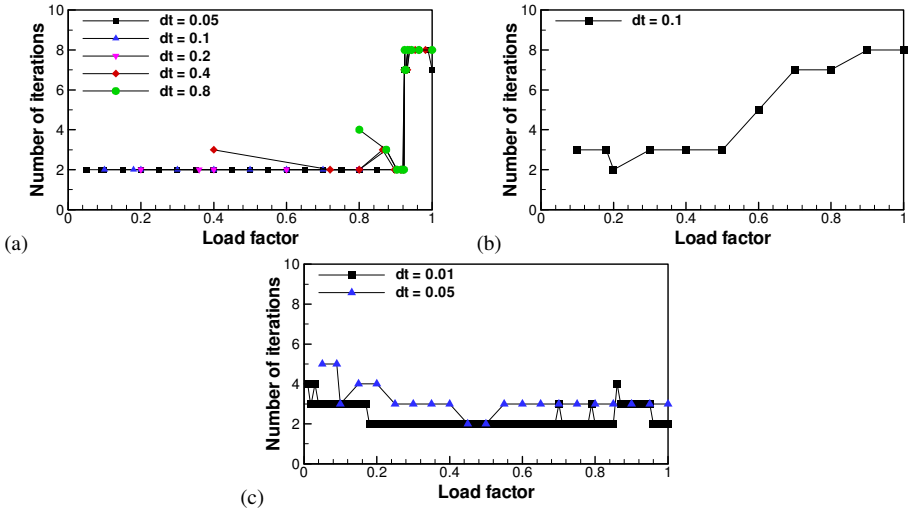

Figure 8. Computational performance obtained by the present model during the physically nonlinear analyses: (a) unit cube; (b) cantilever beam; (c) square plate.

5. CONCLUSIONS

An efficient model for numerical investigations on Nonlinear Solid Mechanics was proposed in this work. The present algorithm presents important characteristics such as the one-point quadrature technique for analytical evaluation of matrices and vector at element level, a corotational formulation for the kinematical description of the continuum and subincrementation procedures for load application and integration of the constitutive equation, where coarse increments defined by the user are automatically adjusted throughout the numerical analysis. The predictions obtained here demonstrated that the present model was able to reproduce the reference results efficiently. In addition, it is important to notice that the subincrementation procedure was also able to deal with applications involving limit points, which usually lead to convergence problems during the iterative process for obtaining the equilibrium state.

6. ACKNOWLEDGEMENTS

The authors would like to thank CNPq for the financial support.

7. REFERENCES

Bathe, K.J., 1996, “Finite Element Procedures”, Prentice Hall, New Jersey, USA.

Belytschko, T. and Bindeman, L.P., 1993, “Assumed strain stabilization of the eight node hexahedral element”, Computer Methods in Applied Mechanics and Engineering, Vol. 105, pp. 225-260.

Belytschko, T., Liu, W.K. and Moran, B., 2000, “Nonlinear Finite Elements for Continua and Structures”, John Wiley & Sons, Chichester, UK.

Braun, A.L. and Awruch, A.M., 2008, “Geometrically non-linear analysis in elastodynamics using the eight-node finite element with one-point quadrature and the generalized-alpha method”, Latin American Journal of Solids and Structures”, Vol. 5, pp. 17-45.

Crisfield, M.A., 1981, “A fast incremental/iterative solution procedure that handles ‘snap-through’”, Computers and Structures, Vol. 13, pp. 55-62.

Duarte Filho, L.A., 2002, “Análise Estática e Dinâmica, Linear e Não-Linear Geométrica, Através de Elementos Hexaédricos de Oito Nós com Um Ponto de Integração”, Dissertação de Mestrado, PPGEC/UFRGS, Porto Alegre.

Duarte Filho, L.A. and Awruch, A.M., 2004, “Geometrically nonlinear static and dynamic analysis of shells and plates using the eight-node hexahedral element with one-point quadrature”, Finite Elements in Analysis and Design, Vol. 40, pp. 1297-1315.

Flanagan, D.P. and Belytschko, T., 1981, “A uniform strain hexahedron and quadrilateral with orthogonal hourglass control”, International Journal for Numerical Methods in Engineering, Vol. 17, pp. 679-706.

Hu, Y-K. and Nagy, L.I., 1997, “A one-point quadrature eight-node brick element with hourglass control”, Computers and Structures, Vol. 65, pp. 893-902.

Liu, W.K., Guo, Y., Tang, S. and Belytschko, T., 1998, "A multiple-quadrature eight-node hexahedral finite element for large deformation elastoplastic analysis", Computer Methods in Applied Mechanics and Engineering, Vol. 154, pp. 69-132.

Memon, B.A. and Su, X., 2004, "Arc-length technique for nonlinear finite element analysis", Journal of Zhejiang University Science, Vol. 5, pp. 618-628.

Owen, D.R.J. and Hinton, E., 1980, "Finite Elements in Plasticity: Theory and Practice", Pineridge Press, Swansea, UK.

Reese, S., 2005, "On physically stabilized one-point finite element formulation for three-dimensional finite elasto-plasticity', Computer Methods in Applied Mechanics and Engineering, Vol. 194, pp. 4685-4715.

Riks, E., 1972, "The application of Newton's method to the problem of elastic stability", Journal of Applied Mechanics, Vol. 39, pp. 1060-1065.

Riks, E., 1979, "An incremental approach to the solution of snapping and buckling problems", International Journal of Solid and Structures", Vol. 15, pp. 529-551.

Schmidt, D., 2006, "Análise Elastoplástica com Não-Linearidade Geométrica de Estruturas Através de Elementos Hexaédricos Tri-Lineares com Um Ponto de Integração", Dissertação de Mestrado, PPGEC/UFRGS, Porto Alegre.

Sloan, S.W. and Abbo, A.J., 1999, "Biot consolidation analysis with automatic time stepping and error control. Part 1: theory and implementation", International Journal for Numerical and Analytical Methods in Geomechanics, Vol. 23, pp. 467-492.

Sloan, S.W., Abbo, A.J. and Sheng, D., 2001, "Refined explicit integration of elastoplastic models with automatic error control", Engineering Computations, Vol. 18, pp. 121-154.

Souza Neto, E.A., Peric´, D. and Owen, D.R.J., 2008, "Computational Methods for Plasticity: Theory and Applications", John Wiley & Sons, Chichester, UK.

Wempner, G.A., 1971, "Discrete approximation related to nonlinear theories of solids", International Journal of Solids and Structures, Vol. 7, pp. 1581-1599.

8. RESPONSIBILITY NOTICE

The authors are the only responsible for the printed material included in this paper.